Pauli paramagnetism of triplet Cooper pairs in a nematic superconductor

D. A. Khokhlov[1,2,3] and R. S. Akzyanov[1,2,4]
[1]*Dukhov Research Institute of Automatics, 127055 Moscow, Russia*
[2]*Moscow Institute of Physics and Technology, Dolgoprudny, 141700 Moscow Region, Russia*
[3]*National Research University Higher School of Economics, 101000 Moscow, Russia*
[4]*Institute for Theoretical and Applied Electrodynamics, Russian Academy of Sciences, 125412 Moscow, Russia*

(Received 17 September 2021; revised 25 November 2021; accepted 16 December 2021; published 29 December 2021)

We investigate the response of a doped topological insulator Bi_2Se_3 with spin-triplet nematic superconductivity to external magnetization. We calculate the Zeeman part of the magnetic susceptibility for nematic and chiral superconducting phases near T_c in the Ginzburg-Landau formalism. The superconducting order parameter from the E_u representation has nontrivial coupling with the transversal Zeeman field that results in a paramagnetic response to magnetization. The topology of a Fermi surface has a strong influence on magnetic susceptibility. The Lifshitz transition from a closed to open Fermi surface eventually leads to a phase transition from the nematic to chiral phase. At the transition point, magnetic susceptibility diverges. Also, we study the effects of the electron-electron interaction on the competition between nematic and chiral phases. We find that in a real system, electron-electron interaction can drive the nematic to chiral phase only in the vicinity of the phase transition. We compare our results with the existing experimental data.

DOI: 10.1103/PhysRevB.104.214514

I. INTRODUCTION

Several years ago topological superconductivity in the bulk of the doped topological insulator (TI) $A_xBi_2Se_3$ was discovered [1–3]. Dopant atom A can be Cu [1–7], Sr [8–13], or Nb [14–17]. The superconducting phase in these materials shows C_2 rotational symmetry that breaks the C_3 symmetry of the normal state. Such rotational symmetry breaking was observed in measurements of specific heat [5], magnetic resonance [16], the in-plane upper critical field [10,12], and the vortex core form [6]. Observation of nuclear magnetic resonance indicates the spin-triplet character of this superconductivity [7].

Such C_2 rotational symmetry is possible due to the realization of the superconducting vector order parameter that belongs to the E_u representation of the crystalline D_{3d} point group [18,19]. One possible solution within such a representation is a nematic order parameter that is a two-component real vector $\boldsymbol{\eta} = \eta(\cos\theta; \sin\theta)$. The direction of this vector is associated with the nematicity axis. The orientation of the nematicity axis shows the direction of twofold symmetry breaking [11,20]. The nematic order parameter brings several interesting features such as vestigial nematic order [21], surface Andreev bound states [22], the unconventional Higgs mode [23], and quasiparticle interference [24,25].

Another possible solution for the order parameter is called chiral and corresponds to the vector with an imaginary component $\boldsymbol{\eta} \propto (1; \pm i)$. This order parameter spontaneously breaks time-reversal symmetry, keeping rotational crystalline symmetry intact [26]. In $Nb_xBi_2Se_3$ such spontaneous breaking of the time-reversal symmetry was found [14]. A muon spin rotational experiment showed time-reversal symmetry breaking in the $Sr_{0.1}Bi_2Se_3$ superconductor [13]. However, another study on $Nb_xBi_2Se_3$ showed the presence of time-reversal symmetry in the superconducting phase [15–17]. Theoretical calculations predict the chiral phase is the ground state in two-dimensional (2D) films of doped Bi_2Se_3 [26,27], while in a three-dimensional (3D) system with a closed Fermi surface, the nematic phase has lower free energy than the chiral state [28–30]. Experimentally, the Fermi surface of doped Bi_2Se_3 with superconductivity has the topology of an open cylinder [31,32], which is an intermediate case between 2D and 3D Fermi surfaces. This transition to the open Fermi surface leads to the phase transition from the nematic to chiral phase [33].

Near the critical temperature, the physical properties of the superconducting state are described by the Ginzburg-Landau (GL) functional, which for the nematic superconductor was obtained in Refs. [19,20]. One of the interesting features of this functional is the coupling between the first power of magnetization and the superconducting order parameter. Such coupling can lead to the transition from the nematic to chiral state with spontaneous magnetization [34]. It was predicted that the transition from the nematic to chiral state occurs upon doping by magnetic ions [28,29].

Magnetization measurements show the presence of the diamagnetic Meissner effect [17]. A muon spin rotational (μSR) experiment can be used to determine local magnetic moments in superconductors [35–38]. A recent μSR experiment did not find time-reversal breaking in superconducting $Nb_{0.25}Bi_2Se_3$ in the absence of magnetic field [17]. However, μSR shows that the superconducting state has an additional paramagnetic magnetization compared to the normal state in the magnetic field. In this work, we show how nontrivial coupling between magnetization and the nematic superconductivity can explain such a paramagnetic response.

In this paper, we calculate the magnetic susceptibility of the nematic superconductor near the critical temperature T_c.

We start with the microscopic derivation of the GL free energy of the doped topological insulator with the open Fermi surface and finite magnetization that is induced by the magnetic field following the common procedure [20,28,29]. We solve GL equations for the order parameter and find that the magnetic field influences the form of the order parameter for the ground state. We calculate the ground-state free energy as a function of magnetic field. Using this free energy, we find that in both nematic and chiral states a paramagnetic contribution to the magnetic susceptibility exists in the system. We interpret this phenomenon as a Pauli paramagnetism of spin-1 Cooper pairs of the nematic superconductor. Such magnetic susceptibility diverges near the transition from the nematic to the chiral state. In addition, we show that coupling between magnetism and superconductivity is rather weak and electron-electron interaction cannot cause the phase transition between nematic and chiral superconductivity.

This paper is organized as follows: in Sec. II we describe the normal and superconducting states in the presence of an external Zeeman field and calculate GL coefficients. Section III is dedicated to the Zeeman susceptibility of the superconductor. In Sec. IV we consider the possibility of the phase transition due to electron-electron interaction. We discuss and summarize the obtained results in Sec. V.

II. MODEL

A. Normal phase

We describe bulk electrons in a doped topological insulator in the Bi_2Se_3 family by a low-energy $\mathbf{k}\cdot\mathbf{p}$ two-orbital Hamiltonian [39]:

$$\hat{H}_0(\mathbf{k}) = -\mu + m\sigma_z + v_z k_z \sigma_y + v(k_x s_y - k_y s_x)\sigma_x, \qquad (1)$$

where μ is the chemical potential, $2m$ is a single-electron gap at the zero chemical potential, and Fermi velocities v and v_z describe motion in the $(\Gamma K;\Gamma M)$ plane and along the ΓZ direction, respectively. Pauli matrices s_i act in spin space, while matrices σ_i act in the space of Bi and Se orbitals $\mathbf{p} = (P^1, P^2)$, where $i = \{x, y, z\}$ and Planck's constant $\hbar = 1$. The Hamiltonian (1) obeys time-reversal symmetry $\hat{\mathcal{T}}\hat{H}_0(\mathbf{k})\hat{\mathcal{T}}^{-1} = \hat{H}_0(-\mathbf{k})$, where $\hat{\mathcal{T}} = is_y\hat{K}$, $\hat{\mathcal{T}}^2 = -1$ is the time-reversal operator and $\hat{K}$ provides complex conjugation. Also, this Hamiltonian has inversion symmetry $\hat{P}\hat{H}_0(\mathbf{k})\hat{P} = \hat{H}_0(-\mathbf{k})$, where $\hat{P} = \sigma_z$ and $\hat{P}^2 = 1$ is the operator of the inversion [39]. Angle-resolved photoemission spectroscopy and measurements of Shubnikov–de Haas oscillations show that the Fermi surface in doped Bi_2Se_3 is open in the ΓZ direction [31,32]. An increase in the chemical potential by doping transforms the closed ellipsoid Fermi surface of undoped samples to a corrugated cylinder Fermi surface of doped samples. For a high chemical potential, dispersion in the z direction disappears, and the system becomes quasi-2D. We introduce a finite length of the 001 lattice constant c into the model. Momentum is bounded by the Brillouin zone's (BZ) size $|k_z| < \pi/c$, or in elliptical coordinates $(vk_x, vk_y, v_z k_z)$ the polar angle stays in the range $\theta \in [\theta_0; \pi - \theta_0]$, where we define the cutoff angle θ_0 as follows:

$$\cos(\theta_0) = \min\left(1, \frac{\pi v_z}{c\sqrt{\mu^2 - m^2}}\right). \qquad (2)$$

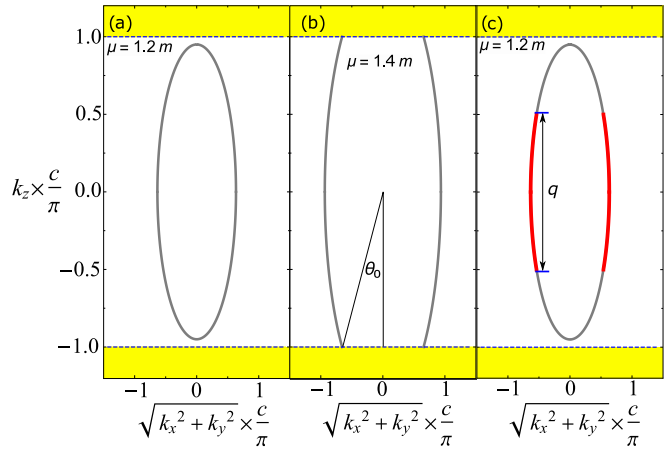

FIG. 1. Fermi surface before and after the Lifshitz transition in dimensionless coordinates. The dashed blue line gives the boundaries of the first BZ (white background) and second BZ (yellow background). (a) The gray curve gives the closed Fermi surface at $\mu = 1.2\,\mathrm{m}$. (b) The gray line gives the open Fermi surface at $\mu = 1.4\,\mathrm{m}$; the cutoff angle θ_0 is defined by Eq. (2). (c) The same Fermi surface as in (a), where parts of the Fermi surface with $|k_z| < q/2$ are highlighted by thick red lines. In these red sheets of the Fermi surface, the electron-phonon coupling is the strongest; see Ref. [41] for details.

In this model, the Fermi surface is closed at a low chemical potential μ. When the chemical potential reaches a critical value $\mu_{\mathrm{LT}} = \sqrt{\pi^2 v_z^2/c^2 - m^2}$, the Fermi surface reaches the boundary of the first BZ and changes topology from ellipsoid to open cylinder, that is, the Lifshitz transition (LT) [40]. We show closed and open Fermi surfaces in Figs. 1(a) and 1(b), respectively.

An experiment with inelastic neutron scattering [41] showed the linewidth of phonon spectra has a singularity for phonon momentum $\mathbf{q}$ oriented along the ΓZ direction while $q \to 0$. The attraction between electrons with momenta $\mathbf{k}$ and $-\mathbf{k}$ in the Cooper channel occurs only for electrons whose k_z components are close enough to each other. Thus, only electrons with momentum $|k_z| < q/2$ participate in superconducting pairing. This singular coupling can be modeled by the Heaviside step function $\theta(q - 2k_z)$, and the Fermi surface where Cooper pairs can be formed is effectively cut off. This new effective Fermi surface has the topology of an open cylinder (see Fig. 1).

B. Superconducting phase

We describe superconductivity in the Nambu II basis, where the wave function is

$$\Psi_{\mathbf{k}} = (\phi^t_{\mathbf{k}}, -i\phi^\dagger_{\mathbf{k}} s_y)^t, \qquad (3)$$

where $\phi_{\mathbf{k}} = (\phi_{\uparrow,1,\mathbf{k}}, \phi_{\downarrow,1,\mathbf{k}}, \phi_{\uparrow,2,\mathbf{k}}, \phi_{\downarrow,2,\mathbf{k}})^t$, the symbol t indicates transpose, and the symbol † indicates the Hermitian conjugate. Operator $\phi^{(\dagger)}_{\uparrow(\downarrow),\sigma,\mathbf{k}}$ annihilates (creates) electrons with up (down) spin on the orbital $\sigma = P^1, P^2$ with momentum $\mathbf{k}$. The superconducting order parameter from the E_u representation of the D_{3d} crystalline point group has the

TABLE I. GL coefficients A, B_1, B_2, g, and a for systems with different Fermi surfaces and different magnetic interactions. The second column describes the 3D system with a closed FS. Coefficients in the quasi-2D system are shown in third column. The fourth column gives the general case of an open FS. Coefficient $j = \frac{2}{\pi}e^c$, where c is the Euler-Mascheroni constant and ζ is the Riemann zeta function.

GL coefficient	$\theta_0 = 0$: closed FS	$\theta_0 = \pi/2$: cylindrical FS	$0 < \theta_0 < \pi/2$: open FS
A	$\frac{\sqrt{\mu^2-m^2}^3(T-T_c)}{3\pi^2\mu T_c v^2 v_z}$	$\frac{(\mu^2-m^2)(T-T_c)}{4\pi c\mu T_c v^2}$	$\frac{\sqrt{\mu^2-m^2}^3(T-T_c)\cos(\theta_0)[7+\cos(2\theta_0)]}{24\pi^2\mu T_c v^2 v_z}$
B_1	$\frac{7\zeta(3)\sqrt{\mu^2-m^2}^5}{30\pi^4 T_c^2\mu^3 v^2 v_z}$	$\frac{21\zeta(3)(\mu^2-m^2)}{128\pi c T_c^2\mu^3 v^2}$	$\frac{7\zeta(3)\cos(\theta_0)\sqrt{\mu^2-m^2}^5[427+76\cos(2\theta_0)+9\cos(4\theta_0)]}{15360\pi^2 T_c^2\mu^3 v^2 v_z}$
B_2	$\frac{7\zeta(3)\sqrt{\mu^2-m^2}^5}{60\pi^4 T_c^2\mu^3 v^2 v_z}$	$-\frac{7\zeta(3)(\mu^2-m^2)}{128\pi c T_c^2\mu^3 v^2}$	$\frac{7\zeta(3)\cos(\theta_0)\sqrt{\mu^2-m^2}^5[71+188\cos(2\theta_0)-3\cos(4\theta_0)]}{15360\pi^2 T_c^2\mu^3 v^2 v_z}$
g_f	$\frac{\sqrt{\mu^2-m^2}}{6\pi^2\mu^2 v^2 v_z}[3m^2\ln(\frac{j\omega_D}{T_c})+2(m^2-\mu^2)]$	$\frac{1}{2\pi c v^2\mu^2}\times[m^2+(m^2-\mu^2)\ln(\frac{j\omega_D}{T_c})]$	$\frac{\sqrt{\mu^2-m^2}\cos(\theta_0)}{6\pi^2 v^2 v_z\mu^2}\times\{m^2[3-\cos^2(\theta_0)+3\ln(\frac{j\omega_D}{T_c})]$ $-\mu^2[2\cos^2\theta_0+3\sin^2\theta_0\ln(\frac{j\omega_D}{T_c})]\}$
g_a	$\frac{m\sqrt{\mu^2-m^2}}{6\pi^2\mu^3 v^2 v_z}\times[3\mu^2\ln(j\omega_D/T_c)+\mu^2-m^2]$	$\frac{m\sqrt{\mu^2-m^2}}{2\pi c v^2\mu}$	$-\frac{m\sqrt{\mu^2-m^2}\cos(\theta_0)}{6\pi^2 v^2 v_z\mu^3}\times(m^2\cos^2(\theta_0)$ $-\mu^2[2-\cos(2\theta_0)+3\cos^2\theta_0\ln(\frac{j\omega_D}{T_c})])$
$a_{f,z}$	$-\frac{\sqrt{\mu^2-m^2}(2m^2+\mu^2)}{12\pi^2 v^2 v_z\mu}$	$-\frac{m^2}{4\pi v^2 c\mu}$	$-\frac{\sqrt{\mu^2-m^2}\cos(\theta_0)[5m^2+\mu^2+\cos(2\theta_0)(\mu^2-m^2)]}{24\pi^2 v^2 v_z\mu}$
$a_{a,z}$	$-\frac{\sqrt{\mu^2-m^2}(m^2+2\mu^2)}{12\pi^2 v^2 v_z\mu}$	$-\frac{\mu}{4\pi v^2 c}$	$-\frac{\sqrt{\mu^2-m^2}\cos(\theta_0)[m^2+5\mu^2-\cos(2\theta_0)(\mu^2-m^2)]}{24\pi^2 v^2 v_z\mu}$
$a_{a,f}$	$\frac{m}{\pi^2\mu v^2 v_z}$	$\frac{m}{\pi c\mu\sqrt{\mu^2-m^2}v^2}$	$\frac{m\cos(\theta_0)}{\pi^2\mu v^2 v_z}$

following matrix structure [26]:

$$\hat{\Delta} = \eta_x s_x\sigma_y(\tau_x + i\tau_y) + \eta_x^* s_x\sigma_y(\tau_x - i\tau_y) + \eta_y s_y\sigma_y(\tau_x + i\tau_y) + \eta_y^* s_y\sigma_y(\tau_x - i\tau_y). \quad (4)$$

The superconducting term depends on two components of vector order parameters $\eta_x = \eta\sin(\alpha)e^{i\phi_1}$ and $\eta_y = \eta\cos(\alpha)e^{i\phi_2}$, where $\phi = \phi_1 - \phi_2$. Matrices τ_i acts in electron-hole space. We assume that only the electrons in the Debye window participate in the superconductivity $-\omega_D < \epsilon_{\mathbf{k}} < \omega_D$, where $\epsilon_{\mathbf{k}}$ is the band's dispersion of the Hamiltonian (1). This order parameter violates inversion symmetry of the normal state.

The Bogoliubov–de Gennes (BdG) Hamiltonian in the Nambu II basis is [18]

$$\hat{H}_{\mathrm{BdG}}(\mathbf{k}) = \tau_z\hat{H}_0(\mathbf{k}) + \hat{\Delta}. \quad (5)$$

We find the GL free energy from microscopic theory as [20,28,29]

$$F = F_0 - T\sum_\omega\int\frac{d\mathbf{k}^3}{(2\pi)^3}\mathrm{Tr}[\ln(1-\hat{G}_0\hat{\Sigma})], \quad (6)$$

where $F_0 = -T\sum_\omega\int\frac{d\mathbf{k}^3}{(2\pi)^3}\mathrm{Tr}[\ln(\hat{G}_0^{-1})]$ is the free energy of a normal state and $\hat{\Sigma}$ is the self-energy. The matrix $\hat{G}_0 = (i\omega - \hat{H}_0)^{-1}$ is the Matsubara Green's function in the Nambu II basis, and the fermionic Matsubara frequency $\omega = (2n+1)\pi T$, where n is an integer. We take the trace $\mathrm{Tr}[\cdot]$ over spin, orbital, and electron-hole degrees of freedom. Then we expand the logarithm from Eq. (6) into a Taylor series $\ln(1-\hat{G}_0\hat{\Sigma}) = -\sum_n\frac{(\hat{G}_0\hat{\Sigma})^n}{n}$ in powers of the perturbation $\hat{\Sigma}$ and combine the terms of the series in powers of order parameters. The calculated GL coefficients are given in Table I. Similar calculations were provided in Refs. [26,28,29].

We start from $\hat{\Sigma} = \hat{\Delta}$ and obtain the superconducting part of the GL free energy [26] up to terms $\propto\eta^4$,

$$F_{\mathrm{sc}}(\eta_x,\eta_y) = A(|\eta_x|^2+|\eta_y|^2) + B_1(|\eta_x|^2+|\eta_y|^2)^2 + B_2|\eta_x^*\eta_y - \eta_x\eta_y^*|^2. \quad (7)$$

The coefficient $A \propto (T - T_c)$ changes sign from positive to negative under cooling from a temperature above T_c to a temperature under T_c, inducing the superconducting phase transition [26].

In the chiral phase expression $|\eta_x^*\eta_y - \eta_x\eta_y^*| = \eta^2$, while in the nematic phase this expression is zero. Thus, the free energy of the chiral phase has an additional term, $B_2\eta^4$. Therefore, in the system with positive $B_2 > 0$, the nematic phase is the ground state, while negative $B_2 < 0$ promotes the chiral phase. The sum of coefficients $B_1 + B_2$ is always positive. Direct calculations using the model with an infinite Brillouin zone and the Hamiltonian (1) show $B_2 > 0$ in the 3D system [28] and $B_2 < 0$ in the 2D case [27].

In the absence of magnetism, the nematic phase has a two-component vector order parameter with real components $\boldsymbol{\eta} = \eta(\cos\alpha;\sin\alpha)$. In the chiral phase the order parameter is a two-component vector again, with one real component and one purely imaginary component $\boldsymbol{\eta} = \frac{\eta}{\sqrt{2}}(1;\pm i)$, which breaks time-reversal symmetry.

We calculate coefficient B_2 for an arbitrary lattice constant c in a model with a finite BZ. The results are given in Table I. The coefficient B_2 is plotted as a function of the Fermi energy μ in Fig. 2 for models with finite and infinite BZs. The Fermi surface is closed at low chemical potential even when the BZ is finite and both models are the same. In the model with an infinite BZ, coefficient $B_2 > 0$ grows with an increase in Fermi energy. Thus, the nematic order parameter has lower energy than the chiral one. The Lifshitz transition occurs at

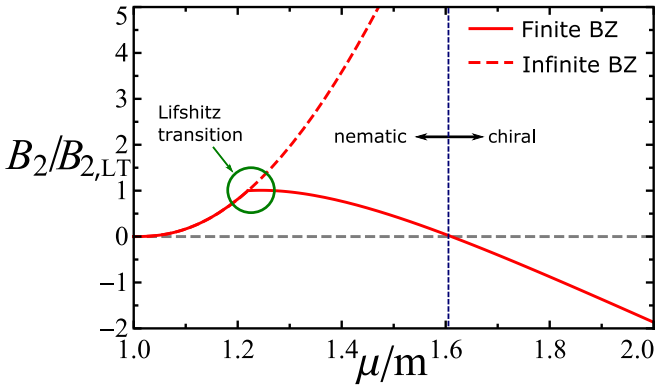

FIG. 2. GL coefficient $B_2(\mu)$ in units of $B_{2,\mathrm{LT}}$ at the Lifshitz transition point vs the dimensionless chemical potential μ/m. The solid red curve corresponds to B_2 calculated in a model with a finite BZ. The dashed red curve corresponds to B_2 calculated in the model with an infinite BZ. The dashed gray horizontal line corresponds to $B_2 = 0$. The vertical dashed blue line shows the transition between the nematic phase with $B_2 > 0$ and the chiral phase with $B_2 < 0$.

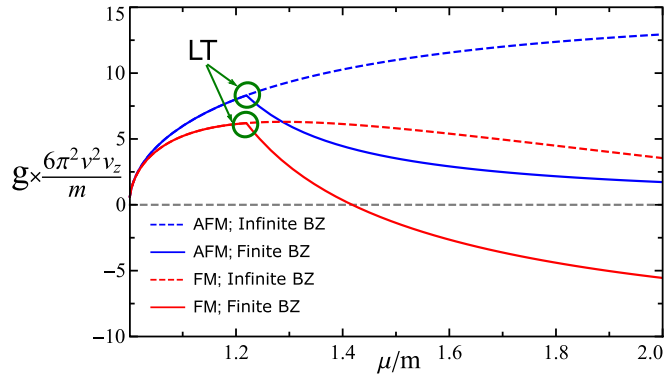

FIG. 3. GL coefficients $g_f(\mu)$ and $g_a(\mu)$ in units of $\frac{m}{6\pi^2v^2v_z}$ versus the dimensionless chemical potential μ/m. Red curves correspond to ferromagnetic coupling g_f, while blue curves correspond to antiferromagnetic coupling g_a. Solid lines correspond to calculations in a model with a finite BZ. Dashed curves correspond to calculations in a model with an infinite BZ. The dashed gray line indicates the zero level. The green circles mark the Lifshitz transition.

$\mu_{\mathrm{LT}} = \sqrt{\frac{\pi^2v_z^2}{c^2} + m^2}$ in the model with a finite BZ and leads to a decrease in B_2. This coefficient reaches zero at the point

$$\mu^* = \sqrt{\frac{v_z^2\pi^2}{c^2\cos^2(\theta_0^*)} + m^2}, \tag{8}$$

where the angle $\theta_0^* \approx 0.985$ does not depend on any parameters. The critical chemical potential μ^* indicates the phase transition between the nematic and chiral superconductivities. In all numerical calculations we set superconducting critical temperature $T_c = 10^{-3}m$, in-plane velocity $v = 1/3mc$, and ΓZ velocity $v_z = \frac{2}{3}v$. This choice of parameters is based on the values $m \approx 0.3$ eV, $v \approx 3$ eV Å, and $v_z \approx 2$eV Å, which are taken from Ref. [39]; $T_c \approx 3$ K was measured in Ref. [17], and the lattice constant $c = 30$ Å (the experimental value is $c = 28.64$Å [42]).

C. Coupling between the magnetism and superconductivity

In the presence of transversal magnetic field electrons in doped Bi_2Se_3 experience orbital-dependent Zeeman magnetization. We decompose this magnetization into ferromagnetic (FM) and antiferromagnetic (AFM), with corresponding Landé factors β_f and β_a (see Ref. [39]) and write it down as

$$\hat{\Sigma}_m = \mu_B\beta_f H s_z + \mu_B\beta_a H s_z\sigma_z. \tag{9}$$

Magnetization order with the spin-orbital structure $s_\alpha\sigma_\beta$, with $\alpha, \beta = \{0, x, y, z\}$, that is different from Eq. (9) does not couple with superconductivity in the lowest order of GL expansion. Thus, we focus on the these two magnetic perturbations that couple with the superconductivity in the lowest order.

We calculate the free energy via Eq. (6), where the perturbation is $\hat{\Sigma} = \hat{\Sigma}_m + \hat{\Delta}$. We expand $\ln(1 - \hat{G}_0\hat{\Sigma})$ in powers of H and η up to $O(\hat{\Sigma}^2)$. The free energy receives additional terms [28,29],

$$F_\alpha(H, \eta_x, \eta_y) = -2ig_\alpha\mu_B\beta_\alpha H(\eta_x^*\eta_y - \eta_x\eta_y^*) + a_\alpha(\mu_B\beta_\alpha H)^2, \tag{10}$$

$$F_m(H) = a_m\beta_f\beta_a\mu_B^2H^2, \tag{11}$$

where $\alpha = \{f, a\}$ refers to FM or AFM terms. Constants a_f, a_a, and a_m describe the response of the normal state to a transverse magnetization (see Table I). We combine terms $\propto H^2$ into one effective term, $a_{\mathrm{eff}}\mu_B^2H^2 = (a_f\beta_f^2 + a_a\beta_a^2 + a_m\beta_f\beta_a)\mu_B^2H^2$.

Coefficients g_f and g_a describe the coupling between the magnetism and superconductivity. Note that in-plane magnetization does not produce such terms. We calculate these coefficients in models with finite and infinite BZs (see Fig. 3). The ferromagnetic coefficient g_f changes sign with the increase of the chemical potential, while the antiferromagnetic coefficient g_a is always positive. According to the expression for g_f at the arbitrary geometry of the Fermi surface given in Table I, it changes to $g_f = 0$ if $\cos^2(\theta_0^{**}) = \frac{3(\ln(j\omega/T)(m^2-\mu^2)+m^2)}{-3\mu^2\ln(j\omega/T)+2\mu^2+m^2}$. At this point coupling between the superconductivity and FM perturbation disappears. The total coupling between the Zeeman field and superconductivity is described by the effective coefficient $g_{\mathrm{eff}} = \beta_f g_f + \beta_a g_a$. We plot $g_{\mathrm{eff}}(\mu)$ in Fig. 4. The coefficient g_{eff} is negative at low chemical potential since both FM and AFM Landé factors are negative. Then g_{eff} changes sign from negative to positive at some value of the Fermi energy. The zero point of g_{eff} occurs at a higher chemical potential than the zero point of g_f in the model with an open FS. In numerical calculations we set Landé factors $\beta_f = -5.3$ and $\beta_a = -7.4$, which were calculated in Ref. [39].

III. MAGNETIC SUSCEPTIBILITY

The response of the superconductor to a magnetic field can be decomposed into a response to the orbital and Zeeman

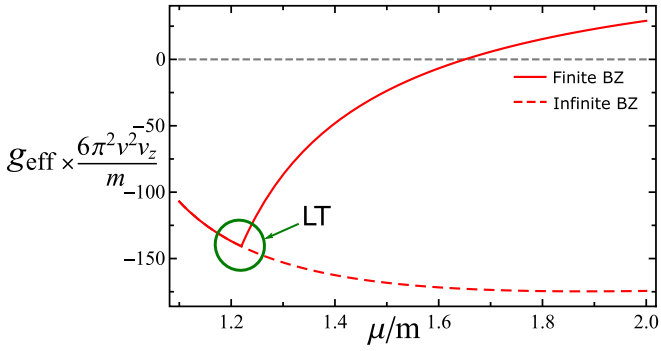

FIG. 4. Effective coupling between superconductivity and Zeeman field $g_{\rm eff}(\mu)$ in units of $\frac{m}{6\pi^2v^2v_z}$ versus the dimensionless chemical potential μ/m. The solid red curve gives $g_{\rm eff}$ calculated in a model with a finite BZ, while the dashed red curve corresponds to calculations in a model with an infinite BZ. The dashed gray curve indicates the zero level. The green circle marks Lifshitz's transition.

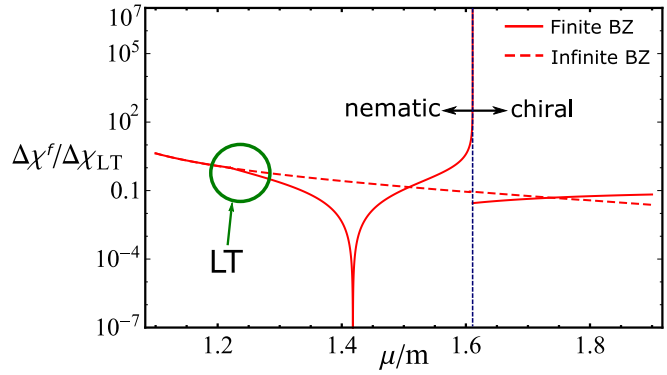

FIG. 5. Jump of the Zeeman susceptibility between superconducting and normal phases $\Delta\chi^f=\chi_{\rm ns}-\chi_n|_{\beta_a=0}$ normalized by its value $\Delta\chi^f_{\rm LT}=\Delta\chi^f(\mu_{\rm LT})$ at the Lifshitz transition point as a function of the dimensionless chemical potential μ/m in the model with only one Landé factor $\beta_f=-5.3$. The red solid curve corresponds to a finite BZ. The red dashed curve corresponds to an infinite BZ. The green circle indicates the Lifshitz transition. The vertical blue dashed line shows the transition between the nematic and chiral phases.

parts of the magnetic field. The orbital part induces Meissner currents and dominates the overall response. The Zeeman part occurs due to a change in the order parameter in the case of finite magnetization. In this paper, we focus only on the second term. The total GL free energy of the E_u superconductor in the Zeeman field is

$$F(H,\eta_x,\eta_y)=F_{\rm sc}(\eta_x,\eta_y)-2ig_{\rm eff}\mu_BH(\eta_x^*\eta_y-\eta_x\eta_y^*)+a_{\rm eff}\mu_B^2H^2. \tag{12}$$

The free energy depends on the value of the complex value components of the order parameter η_x and η_y as well as on the external magnetic field H. We minimize the free energy (12) as a function of $\boldsymbol{\eta}$ and find the equilibrium free energy in the given Zeeman field H. The exact expression for the equilibrium free energy depends on the sign of the B_2 coefficient. We start with the nematic case $B_2>0$. Finite H breaks the time-reversal symmetry, and for the ground state $\sin(2\alpha)\sin(\phi)\propto H$ becomes nonzero; however, we still name this phase nematic [34]. In this case, the free energy is written as

$$F^{\rm nem}_{\rm min}(H)=-\frac{A^2}{4B_1}+a_{\rm eff}\mu_B^2H^2-\frac{g_{\rm eff}^2H^2}{B_2}\left(1-\frac{g_{\rm eff}^2}{B_2a_{\rm eff}}\right) \tag{13}$$

The first term gives the free energy of the nematic phase in zero field. The second term describes the diamagnetism of the normal state. The third term appears due to the coupling between the nematic superconductivity and Zeeman field and describes the superconducting Pauli paramagnetism. We set $(1-\frac{g_{\rm eff}^2}{B_2a_{\rm eff}})\sim(1-\frac{T_c^2}{\mu^2})\simeq 1$ since coupling $g_{\rm eff}$ is small enough. This approximation is valid everywhere except the small neighborhood of the point $B_2=0$. Note that the factor $(1-\frac{g_{\rm eff}^2}{B_2a_{\rm eff}})$ is always positive in Eq. (13). Otherwise, the phase transition from the nematic to chiral phase occurs, and Eq. (13) becomes invalid [34].

The Zeeman part of the magnetic susceptibility is

$$\chi_{\rm ns}=-\frac{\partial^2F^{\rm nem}_{\rm min}(H)}{\partial H^2}=-2a_{\rm eff}\mu_B^2+\frac{2g_{\rm eff}^2}{B_2}. \tag{14}$$

Here the first term corresponds to the Zeeman susceptibility of the normal phase, and the second term arises due to the coupling between the nematic superconductivity and magnetism. The Zeeman susceptibility has a jump under the phase transition between the normal and nematic superconducting phases,

$$\chi_{\rm ns}-\chi_n=\frac{g_{\rm eff}^2\mu_B^2}{2B_2}>0. \tag{15}$$

This jump is relatively small compared to the Pauli paramagnetism of the normal phase χ_n with a small parameter $(\chi_{\rm ns}-\chi_n)/\chi_n=g_{\rm eff}^2/(4B_2a_{\rm eff})\sim(T_c/\mu)^2$. However, this additional paramagnetism is enhanced close to the area $B_2=0$, where the phase transition between the nematic and chiral phases occurs.

Now we minimize the free energy (12) as a function of η_x and η_y for $B_2<0$. In this case the order parameter chiral and free energy is

$$F^{\rm ch}_{\rm min}(H)=\frac{-A^2}{4(B_1+B_2)}+\frac{Ag_{\rm eff}H}{B_1+B_2}-\frac{g_{\rm eff}^2H^2}{B_1+B_2}+a_{\rm eff}\mu_B^2H^2. \tag{16}$$

The jump in susceptibility between the chiral superconducting and normal phases is

$$\chi_{\rm cs}-\chi_n=\frac{g_{\rm eff}^2\mu_B^2}{4(B_1+B_2)}>0, \tag{17}$$

which has no singularities, in contrast to $\chi_{\rm ns}$, since $B_1+B_2>0$.

We calculate the Zeeman susceptibility as a function of the Fermi energy. We consider two different cases when the Zeeman field appears: (i) only in the FM channel with $g_f=-5.3$ and $g_a=0$ (see Fig. 5) and (ii) in both the FM and AFM channels with $g_f=-5.3$ and $g_a=-7.4$ (see Fig. 6). We see that the inclusion of the AFM response in the magnetic field significantly changes the magnetic susceptibility.

In the model with a finite BZ, the Lifshitz transition occurs at $\mu_{\rm LT}\approx 1.25$. Both susceptibilities $\Delta\chi^f$ and $\Delta\chi^{\rm eff}$ diverge

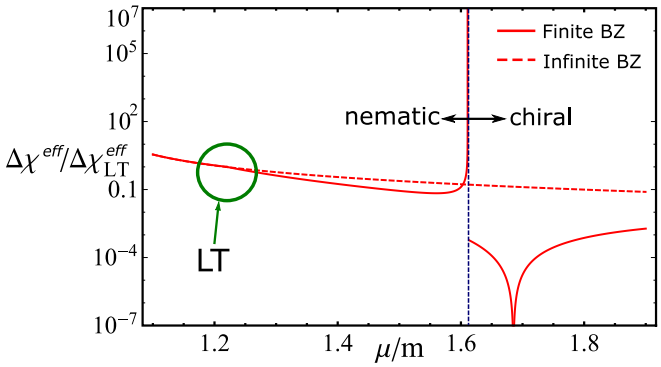

FIG. 6. Jump of the Zeeman susceptibility between superconducting and normal phases $\Delta\chi^{\text{eff}} = \chi_{\text{ns}} - \chi_n$ in units of its value $\Delta\chi^{\text{eff}}_{\text{LT}} = \Delta\chi^f(\mu_{\text{LT}})$ at the Lifshitz transition point as a function of the dimensionless chemical potential μ/m in the model with both Landé factors $\beta_f = -5.3$ and $\beta_a = -7.4$. The red solid curve corresponds to a finite BZ. The red dashed curve corresponds to an infinite BZ. The green circle indicates the Lifshitz transition. The vertical blue dashed line shows the transition between the nematic and chiral phases.

at $\mu \approx 1.6$, where B_2 changes sign and the phase transition from the nematic to chiral phase occurs. These values of the chemical potential depend on the lattice constant c. We consider only $c = 30$ Å for the bulk sample. An increase in the lattice constant c shifts both the Lifshitz transition and the divergence point of the susceptibility to the area where the chemical potential is low.

We also consider a limiting case with $v_z k_c \to 0$. Dispersion along Oz becomes negligible, and the system is a quasi-2D system. We take this limit for each GL coefficient and find these coefficients are finite; see the third column of Table I. We use low-energy $\mathbf{k}\cdot\mathbf{p}$ expansion of the Hamiltonian. Dispersion along Oz can be described by only the linear term even at high energy with enough accuracy. For more details, see the comparison between the linear model and density functional theory calculations in Fig. 4(b) of Ref. [39].

Susceptibility $\Delta\chi^f$ vanishes in the nematic phase at the point $\mu \approx 1.42$, while $\Delta\chi^{\text{eff}}$ vanishes in the chiral phase at the point $\mu \approx 1.68$. This disappearance of susceptibilities occurs at points where g_f and g_{eff} reach a zero value (see Figs. 5 and 6). The model with an infinite BZ system always stays in the nematic phase. Thus, no divergence in susceptibility occurs.

A superconductor with E_u pairing has a triplet structure; that is, Cooper pairs have spin equal to 1 [19]. It can be seen if we write down the order parameter using the second quantization form $\eta_x \propto c_{1\uparrow}c_{2\uparrow} + c_{1\downarrow}c_{2\downarrow}$ and $\eta_y \propto i(c_{1\uparrow}c_{2\uparrow} - c_{1\downarrow}c_{2\downarrow})$, where c_{is} is the operator of the annihilation of the electron on the ith orbital with the spin projection s. We can see that the order parameter represents two Cooper pairs with opposite spins ± 1. Each Cooper pair couples electrons with the same spin on different orbitals. In the presence of the magnetic field the numbers of spin up and spin down Cooper pairs are not equal. Such a spin imbalance influences the form of the order parameter that defines the response to the magnetic field.

The spin density of the system is expressed through a full Green's function as $S_z = -T\sum_\omega \int \frac{d^3k}{(2\pi)^3}\text{Tr}[\hat{G}s_z]$. We expand the superconducting Green's function $\hat{G} \approx \hat{G}_0 + \hat{G}_0\hat{\Delta}\hat{G}_0 + \hat{G}_0\hat{\Delta}\hat{G}_0\hat{\Delta}\hat{G}_0$ in powers of the superconducting order parameter (4) that gives us $S_z = -2ig_{\text{eff}}(\eta_x^*\eta_y - \eta_x\eta_y^*) \propto \sin(2\alpha)\sin(\phi) \propto n_{\uparrow 1}n_{\uparrow 2} - n_{\downarrow 1}n_{\downarrow 2}$, where $n_{s\sigma} = \phi^\dagger_{s\sigma}\phi_{s\sigma}$ is the density of electrons from orbital σ with spin s [19]. We see that the parameter $\sin(2\alpha)\sin(\phi)$ is responsible for the spin imbalance of Cooper pairs. When the order parameter is real, angle $\phi = 0$, the spin density is zero, and the numbers of spin up and spin down Cooper pairs are equal. Turning on the Zeeman field makes the product $\sin(2\alpha)\sin(\phi) \sim H$, and the spin density that arises due to the imbalance between spin up and spin down Cooper pairs becomes $S_z = \frac{g_{\text{eff}}^2\mu_B H}{2B_2} \sim k_F^3\beta_{\text{eff}}^2(\mu_B H/\mu)(T_c/\mu)^2$. Such a spin imbalance decreases the energy of the system in a magnetic field similar to the Pauli paramagnetism of the electrons. Thus, we refer to this effect as Pauli paramagnetism of Cooper pairs.

The average spin density of Cooper pairs in the chiral phase is $S_z = g_{\text{eff}}\eta \approx Ag_{\text{eff}}/(B_1 + B_2) \sim \beta_{\text{eff}}\delta T(T_c k_F^3/\mu^2)$. Therefore, the chiral phase has nonzero magnetization even in the absence of magnetic field. For comparison, the spin density of (i) normal-phase Bi_2Se_3 and (ii) a fully spin polarized metal in the Zeeman field H are of the order of (i) $k_F^3\beta_{\text{eff}}\mu_B H/\mu$ and (ii) k_F^3, respectively. The density of Cooper pairs in the chiral phase increases in the presence of the Zeeman field $\eta = \frac{A+2|g_{\text{eff}}H|}{2(B_1+B_2)}$. Thus, the spin density receives the term $\frac{g_{\text{eff}}^2\mu_B H}{4(B_1+B_2)}$, and the sample receives extra polarization proportional to the Zeeman field H. Therefore, the chiral phase has Zeeman susceptibility despite been fully spin polarized.

IV. PHASE TRANSITION UNDER ELECTRON-ELECTRON REPULSION

Coupling between the magnetic and superconducting order parameters can lead to the emergence of a ferromagnetic or antiferromagnetic phase in the superconducting state. We consider the effects of direct and exchange pointlike electron-electron repulsions. We treat this interaction in the mean-field approach. Only FM and AFM order parameters with spin-orbital structure proportional to s_z and $s_z\sigma_z$ couple with the E_u superconductivity. These order parameters are $M_z = \langle n_\uparrow\rangle - \langle n_\downarrow\rangle$ and $L_z = \langle n_{\uparrow,1}\rangle + \langle n_{\downarrow,2}\rangle - \langle n_{\uparrow,2}\rangle - \langle n_{\downarrow,1}\rangle$, respectively. They appear due to direct interaction. Exchange interaction does not stimulate these order parameters. Here $n_{s\sigma}$ is the local density of electrons with spin s from orbital σ. Both order parameters enter the free energy in the same way as the Zeeman field (10), where factors $\mu_B H\beta_{f(a)}$ should be replaced by $V_{f(a)}M_z(L_z)$. Coefficients $g_{f(a)}$ and a_m do not change, while the coefficient $a_{f(a)} \to a_{f(a),e} = a_{f(a)} + 1/V_{f(a)}$ (see Table I).

Let us consider the system above the superconducting critical temperature T_c. In the presence of only FM electron-electron repulsion, the system stays in the ferromagnetic phase when $a_{f,e} < 0$ and in the paramagnetic phase when $a_{f,e} > 0$. When both FM and AFM orderings are allowed, one more parameter, $4a_{f,e}a_{a,e} - a_m^2$, appears. The negative value of the expression even when both $a_{f,e} > 0$ and $a_{a,e} > 0$ means both the FM and AFM order parameters exist. Otherwise, the order parameters M_z and L_z are zero. We present a magnetic phase diagram in the absence of superconductivity in this simple model in Fig. 7. The three curves in Fig. 7 give three

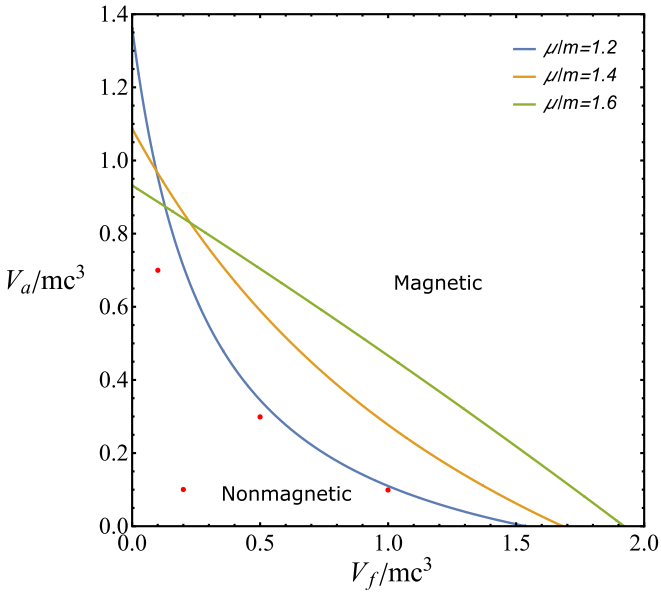

FIG. 7. Phase diagram of the normal phase in coordinates $(\frac{V_f}{mc^3}; \frac{V_a}{mc^3})$ for different values of the chemical potential, $\mu/m = 1.2, 1.4, 1.6$. For any level of μ, magnetic ordering appears above a phase boundary, while below the boundary the system is nonmagnetic. Note that the parameter $mc^3 \approx 8 \times 10^3$eV Å. Red points indicate values of interaction constants V_f and V_a that are used in Fig. 8.

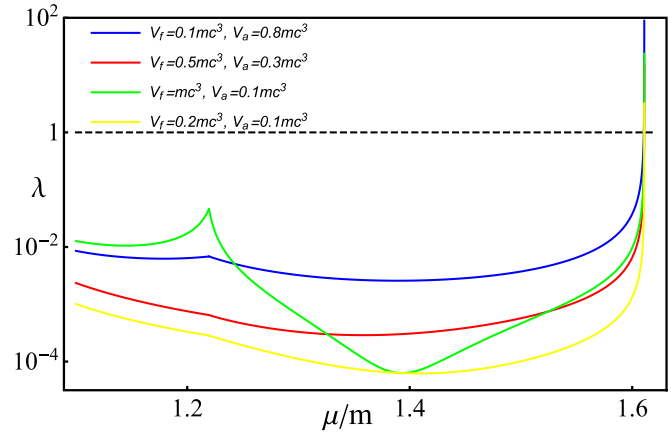

FIG. 8. Parameter λ from Eq. (18) as a function of the dimensionless chemical potential μ/m. The dashed black curve indicates level $\lambda = 1$, where the phase transition from the nematic to chiral phase occurs. Blue, red, and green curves are plotted at different electron-electron repulsion constants from FM $V_f = \{0.1; 0.5; 1; 0.2\}mc^3$ and AFM $V_a = \{0.8; 0.3; 0.1; 0.2\}mc^3$ channels.

phase diagrams at different levels of the chemical potential, $\mu/m = 1.2, 1.4, 1.6$. Each line separates the magnetic (above) and nonmagnetic (below) phases. In all experiments with superconductivity in the bulk of doped Bi_2Se_3, no spontaneous magnetism above T_c was observed. Further, we focus on values of V_f and V_a which give a paramagnetic phase above T_c.

The coupling between the magnetic order parameter and superconductivity can induce the phase transition from the nematic to chiral phase even under $B_2 > 0$. Particularly, when $V_a = 0$, the phase transition occurs when $\frac{g_f^2}{a_{f,e}B_2} > 1$ (see Ref. [34]). Direct calculations show this fraction has order $(T/\mu)^2 \ll 1$. While both FM and AFM order parameters exist, we find a generalized condition on the phase transition between the nematic and chiral states,

$$\lambda = \frac{a_{a,e}g_f^2 - a_m g_f g_a + a_{f,e}g_a^2}{\left(4a_{f,e}a_{a,e} - a_m^2\right)B_2} > 1. \tag{18}$$

The above inequality is similar to the Stoner criterion [43].

We calculate the parameter λ as a function of the chemical potential μ in Fig. 8. Different curves show the behavior of $\lambda(\mu)$ at different electron-electron repulsion constants V_a and V_f. Even at a high value of the repulsion constants, the generalized condition (18) is met only in the narrow neighborhood of the point $B_2 = 0$. Parameter $\lambda \sim 1$ only in a narrow range of chemical potentials even when magnetic electron-electron interaction is strong and the system is close to the magnetic phase transition.

Condition (18) can be met only via fine-tuning of the chemical potential μ and the position of the system in the phase diagram in Fig. 7. (i) The system should stay close to the appearance of the magnetic order parameters even above critical temperature T_c, and (ii) coefficient B_2 should be close to zero (stay close to the phase transition between the nematic and chiral phases). Only when these two conditions are met can we expect electron-electron interaction to stimulate the phase transition between the nematic and chiral phases. The needs of such fine tuning impose strong conditions on electron-electron interactions V_f and V_a as well as at the chemical potential μ. Therefore, the emergence of the chiral phase from the nematic phase under electron-electron interaction in the absence of magnetic ordering in the normal phase seems unlikely.

V. DISCUSSION

Recently, a superconducting powder of $Nb_{0.25}Bi_2Se_3$ was investigated in a μSR experiment [17]. The authors measured the magnetization of a sample at different temperatures in the external magnetic field. In contrast to a previous experiment [14], there the authors found the system has time-reversal symmetry in the absence of a magnetic field. In their Fig. 3(b), the authors of Ref. [17] showed the temperature dependence of magnetization in the superconducting phase counted from magnetization in the normal phase at $T = 5$ K (above T_c). Surprisingly, the magnetic moment of the superconducting phase is higher than in the normal one, which indicates the appearance of an additional paramagnetism associated with superconductivity. We claim that Pauli paramagnetism of triplet Cooper pairs is observed in this experiment. Note that measurements of the magnetic susceptibility of the large monocrystal $Nb_{0.25}Bi_2Se_3$ using a superconducting quantum interference device show a strong diamagnetic response that is expected in superconductors [17].

Typically, superconductors in low magnetic fields demonstrate diamagnetism due to the Meissner effect, which occurs due to the response to an orbital part of a magnetic field [44,45]. In this paper, we focus on the coupling between spin and magnetization and do not take into account Meissner

currents since they were calculated in previous works. Due to rather weak coupling between magnetization and superconductivity, we expect that the diamagnetic susceptibility from the Meissner effect will dominate paramagnetic susceptibility for large samples. However, in a few regimes, the paramagnetic part of the magnetic susceptibility can dominate. The first regime is realized for a thin superconducting film of thickness $d \ll \lambda$, where $\lambda \sim 10^4$ Å is the penetration depth [17]. The film is thin along the Ox or Oy axis, and a magnetic field is applied along Oz. We estimate diamagnetic Meissner susceptibility via the formula for an s-wave superconductor $\chi_M = -\frac{d^2}{48\pi\lambda^2}$. The thickness of the film d should be a least higher than the in-plane lattice constant $a = 4.14$ Å [46], and the factor $(d/\lambda)^2$ can be of the order of 10^{-6}. Such geometry was used to find the Clogston limit [47,48]. Recent studies demonstrated the possibility of growing high-index films of Bi_2Se_3 [49,50]. An in-plane field for such a film has a nonzero z component, which makes it possible to observe the Pauli paramagnetism of Cooper pairs.

The second possible regime is to investigate a 3D sample in a high magnetic field $H \sim H_{c2}$. We again estimate its Meissner diamagnetic susceptibility via the formula for an s-wave superconductor $\chi_M = -\frac{H_{c2}-H}{16\pi\kappa^2}$ [51,52], where the GL constant $\kappa = \lambda/\xi \sim 50$ in doped Bi_2Se_3 [6,17]. In this scenario, a superconducting fraction of a sample is proportional to $H_{c2} - H$, and thus, the paramagnetic susceptibility is suppressed by the same factor, while Meissner diamagnetism is suppressed much more strongly. Note that surface superconductivity appears here. It possibly brings another contribution to the paramagnetism [53].

The third way is based on the presence of a spin imbalance of the Coopers pair in the Zeeman field. The fraction of imbalance is of the order of $(\beta_{\text{eff}}\mu_B H)/\mu \sim 10^{-3}$–$10^{-2}$ (see Sec. III). Therefore, we expect that the supercurrent in such a system is partially spin polarized. Although similar experiments were conducted recently, the topic needs deeper investigation [54].

Magnetism can induce a phase transition between nematic and chiral superconductivity [28,29]. We investigate this phase transition, assuming magnetism appears because of pointlike electron-electron repulsion. The interaction part of the Hamiltonian consists of all four possible c operators, where two operators are creation and the other two are annihilation. Some of these four describe the direct interaction, while the others describe the exchange interaction. We take into account both types of interaction in the mean-field approach. Only order parameters M_z and L_z couple with superconductivity in the lowest order of GL expansion. Thus, we focus on these terms. Direct calculations show the exchange interaction does not contribute to both the M_z and L_z order parameters. We find the general condition of the phase transition (18). Since coupling between magnetism and superconductivity is small, this condition is met only when the system stays close to the magnetic phase transition above T_c and close to phase transition between the nematic and chiral phases below T_c simultaneously. Such requirements impose strong conditions on the electron-electron repulsion constants V_f and V_a as well as on the chemical potential μ. We conclude that in the considered model the electron-electron repulsion is unlikely to induce the phase transition from the nematic to chiral phase. The result of our calculations in the toy model within the mean-field approximation shows the phase transition is suppressed by weak coupling of the superconductivity and magnetism. The role of electron-electron repulsion can be interesting in the context of samples with magnetic ordering above T_c. In such a scenario more accurate calculations are required.

We introduce the finite lattice constant c to our model. Thus, the topology and shape of the Fermi surface can be controlled by the chemical potential μ (see Fig. 1). We show the coefficient $B_2(\mu)$ in Fig. 2 and find that B_2 changes sign from positive to negative at the critical chemical potential (8). Thus, one can induce a phase transition from the nematic to chiral phase via an increase of the chemical potential. Although the limiting case of the system with the pure cylindrical Fermi surface coincides with a single-layer film, our model does not describe an arbitrary several-layer film. A superconducting thin film of doped Bi_2Se_3 was theoretically investigated in Ref. [28]. The authors predicted the appearance of chiral superconductivity in a single-layer film that coincides with our results.

The lattice constant c also affects the shape of the Fermi surface and the sign of B_2 since it appears in Eq. (8). The hopping integral depends on c, and thus, the Fermi velocity $v_z = tc$. A common way to change a lattice constant is to apply hydraulic pressure to the sample. This pressure acts spherically and changes all lattice constants, Fermi velocities v and v_z, and the chemical potential. Moreover, strong pressure causes a structural transition that can destroy the E_u nematic superconductivity [55,56].

In Ref. [32] the evolution of the Fermi surface of Bi_2Se_3 upon doping was investigated. the authors showed that doping increases carrier density, which leads to the transformation of a closed Fermi surface to open. This transformation coincides with the emergence of the superconductivity and occurs at a carrier density of $2 \times 10^{19} \lesssim n \lesssim 10^{20}\,\text{cm}^{-3}$. According to Ref. [31], the Lifshitz transition occurs at carrier density $n = 5 \times 10^{19}\,\text{cm}^{-3}$. In Ref. [4] the authors investigated excessive Cu doping in Bi_2Se_3. They obtained several samples with Cu concentration in the range $0.28 < x < 0.54$. According to Knight shift measurements, the carrier density at $x > 0.37$ strongly increases, which perhaps turns the system to the chiral phase. Thus, the realization of the chiral superconductivity in overdoped samples is possible in such samples. Since doping is nonuniform in general, the macroscopic parts of the superconductor can be in the vicinity of the nematic to chiral phase transitions. Since paramagnetic susceptibility diverges near the transition, such parts can provide a substantial contribution to the susceptibility, which can be used to track the phase transition.

ACKNOWLEDGMENTS

Authors acknowledge support from the Russian Science Foundation under Grant No. 20-72-00030 and partial support from the Foundation for the Advancement of Theoretical Physics and Mathematics "BASIS."

[1] Y. S. Hor, A. J. Williams, J. G. Checkelsky, P. Roushan, J. Seo, Q. Xu, H. W. Zandbergen, A. Yazdani, N. P. Ong, and R. J. Cava, Superconductivity in $Cu_xBi_2Se_3$ and Its Implications for Pairing in the Undoped Topological Insulator, Phys. Rev. Lett. **104**, 057001 (2010).

[2] S. Sasaki, M. Kriener, K. Segawa, K. Yada, Y. Tanaka, M. Sato, and Y. Ando, Topological Superconductivity in $Cu_xBi_2Se_3$, Phys. Rev. Lett. **107**, 217001 (2011).

[3] T. Kirzhner, E. Lahoud, K. B. Chaska, Z. Salman, and A. Kanigel, Point-contact spectroscopy of $Cu_{0.2}Bi_2Se_3$ single crystals, Phys. Rev. B **86**, 064517 (2012).

[4] T. Kawai, C. G. Wang, Y. Kandori, Y. Honoki, K. Matano, T. Kambe, and G. Zheng, Direction and symmetry transition of the vector order parameter in topological superconductors $Cu_xBi_2Se_3$, Nat. Commun. **11**, 235 (2020).

[5] S. Yonezawa, K. Tajiri, S. Nakata, Y. Nagai, Z. Wang, K. Segawa, Y. Ando, and Y. Maeno, Thermodynamic evidence for nematic superconductivity in $Cu_xBi_2Se_3$, Nat. Phys. **13**, 123 (2016).

[6] R. Tao, Y.-J. Yan, X. Liu, Z.-W. Wang, Y. Ando, Q.-H. Wang, T. Zhang, and D.-L. Feng, Direct Visualization of the Nematic Superconductivity in $Cu_xBi_2Se_3$, Phys. Rev. X **8**, 041024 (2018).

[7] K. Matano, M. Kriener, K. Segawa, Y. Ando, and G. Zheng, Spin-rotation symmetry breaking in the superconducting state of $Cu_xBi_2Se_3$, Nat. Phys. **12**, 852 (2016).

[8] Shruti, V. K. Maurya, P. Neha, P. Srivastava, and S. Patnaik, Superconductivity by Sr intercalation in the layered topological insulator Bi_2Se_3, Phys. Rev. B **92**, 020506(R) (2015).

[9] Z. Liu, X. Yao, J. Shao, M. Zuo, L. Pi, S. Tan, C. Zhang, and Y. Zhang, Superconductivity with topological surface state in $Sr_xBi_2Se_3$, J. Am. Chem. Soc. **137**, 10512 (2015).

[10] A. Y. Kuntsevich, M. A. Bryzgalov, V. A. Prudkoglyad, V. P. Martovitskii, Y. G. Selivanov, and E. G. Chizhevskii, Structural distortion behind the nematic superconductivity in $Sr_xBi_2Se_3$, New J. Phys. **20**, 103022 (2018).

[11] A. Y. Kuntsevich, M. A. Bryzgalov, R. S. Akzyanov, V. P. Martovitskii, A. L. Rakhmanov, and Y. G. Selivanov, Strain-driven nematicity of odd-parity superconductivity in $Sr_xBi_2Se_3$, Phys. Rev. B **100**, 224509 (2019).

[12] Y. Pan, A. M. Nikitin, G. K. Araizi, Y. K. Huang, Y. Matsushita, T. Naka, and A. de Visser, Rotational symmetry breaking in the topological superconductor $Sr_xBi_2Se_3$ probed by upper-critical field experiments, Sci. Rep. **6**, 28632 (2016).

[13] P. Neha, P. K. Biswas, T. Das, and S. Patnaik, Time-reversal symmetry breaking in topological superconductor $Sr_{0.1}Bi_2Se_3$, Phys. Rev. Materials **3**, 074201 (2019).

[14] Y. Qiu, K. N. Sanders, J. Dai, J. E. Medvedeva, W. Wu, P. Ghaemi, T. Vojta, and Y. S. Hor, Time reversal symmetry breaking superconductivity in topological materials, arXiv:1512.03519.

[15] C. Kurter, A. D. K. Finck, E. D. Huemiller, J. Medvedeva, A. Weis, J. M. Atkinson, Y. Qiu, L. Shen, S. H. Lee, T. Vojta, P. Ghaemi, Y. S. Hor, and D. J. V. Harlingen, Conductance spectroscopy of exfoliated thin flakes of $Nb_xBi_2Se_3$, Nano Lett. **19**, 38 (2018).

[16] T. Asaba, B. J. Lawson, C. Tinsman, L. Chen, P. Corbae, G. Li, Y. Qiu, Y. S. Hor, L. Fu, and L. Li, Rotational Symmetry Breaking in a Trigonal Superconductor Nb-Doped Bi_2Se_3, Phys. Rev. X **7**, 011009 (2017).

[17] D. Das, K. Kobayashi, M. P. Smylie, C. Mielke, T. Takahashi, K. Willa, J.-X. Yin, U. Welp, M. Z. Hasan, A. Amato, H. Luetkens, and Z. Guguchia, Time-reversal invariant and fully gapped unconventional superconducting state in the bulk of the topological compound $Nb_{0.25}Bi_2Se_3$, Phys. Rev. B **102**, 134514 (2020).

[18] L. Fu and E. Berg, Odd-Parity Topological Superconductors: Theory and Application to $Cu_xBi_2Se_3$, Phys. Rev. Lett. **105**, 097001 (2010).

[19] L. Fu, Odd-parity topological superconductor with nematic order: Application to $Cu_xBi_2Se_3$, Phys. Rev. B **90**, 100509(R) (2014).

[20] J. W. F. Venderbos, V. Kozii, and L. Fu, Identification of nematic superconductivity from the upper critical field, Phys. Rev. B **94**, 094522 (2016).

[21] M. Hecker and J. Schmalian, Vestigial nematic order and superconductivity in the doped topological insulator Cu_x Bi_2Se_3, npj Quantum Mater. **3**, 26 (2018).

[22] L. Hao and C. S. Ting, Nematic superconductivity in $Cu_xBi_2Se_3$: Surface Andreev bound states, Phys. Rev. B **96**, 144512 (2017).

[23] H. Uematsu, T. Mizushima, A. Tsuruta, S. Fujimoto, and J. A. Sauls, Chiral Higgs Mode in Nematic Superconductors, Phys. Rev. Lett. **123**, 237001 (2019).

[24] M. Chen, X. Chen, H. Yang, Z. Du, and H.-H. Wen, Superconductivity with twofold symmetry in $Bi_2Te_3/FeTe_{0.55}Se_{0.45}$ heterostructures, Sci. Adv. **4**, eaat1084 (2018).

[25] D. A. Khokhlov and R. S. Akzyanov, Quasiparticle interference in doped topological insulators with nematic superconductivity, Phys. E (Amsterdam, Neth.) **133**, 114800 (2021).

[26] J. W. F. Venderbos, V. Kozii, and L. Fu, Odd-parity superconductors with two-component order parameters: Nematic and chiral, full gap, and Majorana node, Phys. Rev. B **94**, 180504(R) (2016).

[27] L. Chirolli, Chiral superconductivity in thin films of doped Bi_2Se_3, Phys. Rev. B **98**, 014505 (2018).

[28] L. Chirolli, F. de Juan, and F. Guinea, Time-reversal and rotation symmetry breaking superconductivity in dirac materials, Phys. Rev. B **95**, 201110(R) (2017).

[29] N. F. Q. Yuan, W.-Y. He, and K. T. Law, Superconductivity-induced ferromagnetism and Weyl superconductivity in Nb-doped Bi_2Se_3, Phys. Rev. B **95**, 201109(R) (2017).

[30] R. S. Akzyanov, D. A. Khokhlov, and A. L. Rakhmanov, Nematic superconductivity in topological insulators induced by hexagonal warping, Phys. Rev. B **102**, 094511 (2020).

[31] A. Almoalem, I. Silber, S. Sandik, M. Lotem, A. Ribak, Y. Nitzav, A. Y. Kuntsevich, O. A. Sobolevskiy, Y. G. Selivanov, V. A. Prudkoglyad, M. Shi, L. Petaccia, M. Goldstein, Y. Dagan, and A. Kanigel, Link between superconductivity and a Lifshitz transition in intercalated Bi_2Se_3, Phys. Rev. B **103**, 174518 (2021).

[32] E. Lahoud, E. Maniv, M. S. Petrushevsky, M. Naamneh, A. Ribak, S. Wiedmann, L. Petaccia, Z. Salman, K. B. Chashka, Y. Dagan, and A. Kanigel, Evolution of the Fermi surface of a doped topological insulator with carrier concentration, Phys. Rev. B **88**, 195107 (2013).

[33] L. Yang and Q.-H. Wang, The direction of the d-vector in a nematic triplet superconductor, New J. Phys. **21**, 093036 (2019).

[34] R. S. Akzyanov, A. V. Kapranov, and A. L. Rakhmanov, Spontaneous strain and magnetization in doped topological in-

sulators with nematic and chiral superconductivity, Phys. Rev. B **102**, 100505(R) (2020).

[35] A. J. Drew, C. Niedermayer, P. J. Baker, F. L. Pratt, S. J. Blundell, T. Lancaster, R. H. Liu, G. Wu, X. H. Chen, I. Watanabe, V. K. Malik, A. Dubroka, M. Rössle, K. W. Kim, C. Baines, and C. Bernhard, Coexistence of static magnetism and superconductivity in $SmFeAsO_{1-x}F_x$ as revealed by muon spin rotation, Nat. Mater. **8**, 310 (2009).

[36] E. Morenzoni, B. M. Wojek, A. Suter, T. Prokscha, G. Logvenov, and I. Božović, The Meissner effect in a strongly underdoped cuprate above its critical temperature, Nat. Commun. **2**, 272 (2011).

[37] R. Khasanov, G. Simutis, Y. G. Pashkevich, T. Shevtsova, W. R. Meier, M. Xu, S. L. Bud'ko, V. G. Kogan, and P. C. Canfield, Magnetism and its coexistence with superconductivity in $CaK(Fe_{0.949}Ni_{0.051})_4As_4$: Muon spin rotation/relaxation studies, Phys. Rev. B **102**, 094504 (2020).

[38] D. E. MacLaughlin, D. W. Cooke, R. H. Heffner, R. L. Hutson, M. W. McElfresh, M. E. Schillaci, H. D. Rempp, J. L. Smith, J. O. Willis, E. Zirngiebl, C. Boekema, R. L. Lichti, and J. Oostens, Muon spin rotation and magnetic order in the heavy-fermion compound URu_2Si_2, Phys. Rev. B **37**, 3153 (1988).

[39] C.-X. Liu, X.-L. Qi, H. J. Zhang, X. Dai, Z. Fang, and S.-C. Zhang, Model hamiltonian for topological insulators, Phys. Rev. B **82**, 045122 (2010).

[40] I. Lifshitz, Anomalies of electron characteristics of a metal in the high pressure region, Sov. Phys. JETP **11**, 1130 (1960).

[41] J. Wang, K. Ran, S. Li, Z. Ma, S. Bao, Z. Cai, Y. Zhang, K. Nakajima, S. Ohira-Kawamura, P. Čermák, A. Schneidewind, S. Y. Savrasov, X. Wan, and J. Wen, Evidence for singular-phonon-induced nematic superconductivity in a topological superconductor candidate $Sr_{0.1}Bi_2Se_3$, Nat. Commun. **10**, 2802 (2019).

[42] S. Nakajima, The crystal structure of $Bi_2Te_{3-x}Se_x$, J. Phys. Chem. Solids **24**, 479 (1963).

[43] E. C. Stoner, Collective electron ferromagnetism, Proc. R. Soc. London, Ser. A **165**, 372 (1938).

[44] R. S. Akzyanov, Lifshitz transition in dirty doped topological insulator with nematic superconductivity, Phys. Rev. B **104**, 224502 (2021).

[45] J. Schmidt, F. Parhizgar, and A. M. Black-Schaffer, Odd-frequency superconductivity and Meissner effect in the doped topological insulator Bi_2Se_3, Phys. Rev. B **101**, 180512(R) (2020).

[46] A. Cavallin, V. Sevriuk, K. N. Fischer, S. Manna, S. Ouazi, M. Ellguth, C. Tusche, H. L. Meyerheim, D. Sander, and J. Kirschner, Preparation and characterization of $Bi_2Se_3(0001)$ and of epitaxial FeSe nanocrystals on $Bi_2Se_3(0001)$, Surf. Sci. **646**, 72 (2016).

[47] A. M. Clogston, Upper Limit for the Critical Field in Hard Superconductors, Phys. Rev. Lett. **9**, 266 (1962).

[48] H. Nam, H. Chen, T. Liu, J. Kim, C. Zhang, J. Yong, T. R. Lemberger, P. A. Kratz, J. R. Kirtley, K. Moler, P. W. Adams, A. H. MacDonald, and C.-K. Shih, Ultrathin two-dimensional superconductivity with strong spin–orbit coupling, Proc. Natl. Acad. Sci. USA **113**, 10513 (2016).

[49] Z. Xu, X. Guo, M. Yao, H. He, L. Miao, L. Jiao, H. Liu, J. Wang, D. Qian, J. Jia, W. Ho, and M. Xie, Anisotropic topological surface states on high-index Bi_2Se_3 films, Adv. Mater. **25**, 1557 (2013).

[50] H. Li, S. Yu, Y. Li, A. I. Channa, H. Ji, J. Wu, X. Niu, and Z. Wang, The coherent heteroepitaxy of high-index Bi_2Se_3 thin film on nanofaceted Si(211) substrate, Appl. Phys. Lett. **115**, 041602 (2019).

[51] A. A. Abrikosov, On the magnetic properties of superconductors of the second group, JETP **5**, 1174 (1957).

[52] V. V. Schmidt, in *The Physics of Superconductors*, edited by P. Müller and A. V. Ustinov (Springer, Berlin, 1997).

[53] A. K. Geim, S. V. Dubonos, J. G. S. Lok, M. Henini, and J. C. Maan, Paramagnetic Meissner effect in small superconductors, Nature (London) **396**, 144 (1998).

[54] W. Han, S. Maekawa, and X.-C. Xie, Spin current as a probe of quantum materials, Nat. Mater. **19**, 139 (2019).

[55] A. M. Nikitin, Y. Pan, Y. K. Huang, T. Naka, and A. de Visser, High-pressure study of the basal-plane anisotropy of the upper critical field of the topological superconductor $Sr_xBi_2Se_3$, Phys. Rev. B **94**, 144516 (2016).

[56] Z. Yu, L. Wang, Q. Hu, J. Zhao, S. Yan, K. Yang, S. Sinogeikin, G. Gu, and H. Mao, Structural phase transitions in Bi_2Se_3 under high pressure, Sci. Rep. **5**, 15939 (2015).